Partial Mitigation of global warming through Antarctic Meltwater Anomalies

Craig D Rye[1,2], John Marshall[2], David Rind[1], Gavin A. Schmidt[1], James E Hansen[3]

1 Goddard Institute for Space Studies

2 MIT

3 Columbia University

Abstract

Mechanisms connecting Antarctic Meltwater Anomalies (AAMA) to surface cooling are explored through analysis of climate feedbacks in a coupled climate model. In response to step-changes in meltwater forcing we find that patterns of temperature change are similar to greenhouse gas (GHG) forcing but have opposite sign. The strength of the cooling induced by AAMA relative to the warming from GHGs is described in terms of the efficacy of the respective forcings. We find that AAMA, despite their high latitude location, can generate global surface temperature changes just as more globally distributed climate forcings such as GHGs. Increases in AAMA affect global temperatures first by inducing local cooling, which, if sustained, increases sea-ice extent, reduces atmospheric water vapor and thus atmospheric greenhouse capacity, leading to more widespread surface cooling. Melt rates ranging from current observed levels to extreme possibilities lead to a non-linear response which damps the response to large AAMA. Our results indicate that current and expected melt rates are likely to result in a noticeable near-term amelioration of CO_2-induced warming. AAMA may reduce global surface warming by as much as 10 to 30% by mid-century in plausible meltwater and GHG emission scenarios. Larger meltwater injection is conceivable on longer time scales. Due to non-linearities, such larger melt rates may not yield a response proportionate to

present-day smaller meltwater inputs. We conclude that as this century proceeds, AAMA will be a key player in future climate change.

Introduction

In recent years it has become clear that the discharge of fresh water from glacial melt into the open ocean around Antarctica may be playing an important role in recent climate trends and will be increasingly important for climate change projections (Fig. 1; see, e.g. Rye et al., 2014; 2020, Hansen et al., 2016, Bronselaer et al 2018, Schloesser et al., 2019). However, there are many uncertainties: the rate and geographical distribution of AAMA, pathways and dilution rates of meltwaters as they move from melting ice shelves at the margins into the open ocean, subsequent effects on the upper ocean and sea-ice distributions, air-sea interaction and the response of the atmosphere above. That said, several recent studies indicate that AAMA may be an important 'missing process' in current climate models whose inclusion could significantly improve well-documented coupled model biases and their ability to maintain Antarctic sea ice in a warming world (Fig. 1; e.g. Bronselaer et al 2018, Rye et al., 2020).

Antarctic climate trends are strongly influenced by wind changes. It has been argued that recent Southern Hemisphere climate trends are, directly (Sen Gupta et al., 2009; Kostov et al., 2016; Seviour et al 2016) or indirectly, driven by wind forcing (Abernathy et al., 2016; Haumann et al., 2016). For example, the modelling and observations work of Haumann et al., (2016) and Moorman et al., (2020) suggest that the recent trend in Southern Ocean cooling is driven primarily by changes in wind-driven sea ice transport with glacial fluxes playing a supporting role. However, Kostov et al., (2018) find that winds alone cannot explain the observed cooling trends around Antarctica. Rye et al. 2020 note that AAMA is missing in current models and argue that, when included, can bring modelled climate trends into closer accord with observed trends.

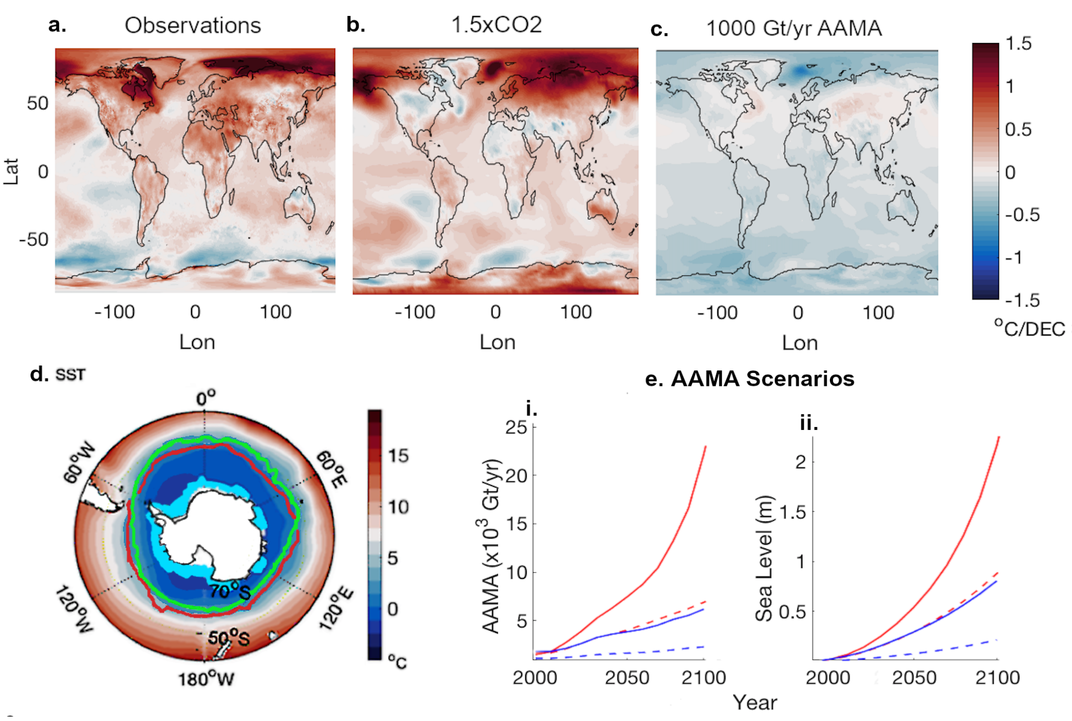

Figure 1 | Observed global surface temperature change and simulated change for CO2 and Antarctic Meltwater Anomaly (AMA) forcings. a. Trend in ERA-5 reanalysis surface temperature 1990-2015. b. Trends in GISS-2.1-G surface temperature 25 years after an abrupt 1.5x increase of CO2. c. Trend in GISS-2.1-G over 25 years following an abrupt 1000 Gt/yr AAMA perturbation experiment; current AAMA forcing is estimated to be 750 Gt/yr (Rye et al., 2020). d. Climatology of GISS-2.1-G Sea Surface Temperature (SST). Redline: GISS-2.1-G Sea Ice extent. Green line: Observed Sea Ice extent. Cyan area: region where AAMA is released in perturbation experiments. e. i.) AAMA scenarios taken from (red) DeConto and Pollard, (2016) and (blue) Golledge et al., (2019). Full lines: RCP *8.5. Dashed lines: RCP:4.5*. ii.) Equivalent sea level change from Antarctic meltwater alone, including both grounded ice and floating ice shelve components.

Here we use the Climate Response Function (CRF) framework (the transient response of key observable indicators to abrupt ‘step’ changes in forcing – see Supplementary Material, A) employed in Rye et al (2020) to explore the efficacy of AAMA in affecting global climate change, enabling us to place AAMA in the context of other drivers, and particularly GHGs. As summarised in Fig.1(a-c), in response to step-changes in AAMA and an increased GHG forcing, we find that spatial patterns of temperature response closely mirror that of GHG, but have the opposite sign. Here the response is summarised in terms of CRFs for key variables such as sea ice cover, surface temperature, greenhouse capacity and shortwave radiation anomaly at the top of the atmosphere.

Modeled response to Antarctic Meltwater Anomalies

A number of studies have recently explored the response of the Southern Ocean (SO) to perturbations in AAMA. Introduction of anomalous glacial melt simultaneously improves multiple SO trends consistent with observations (particularly in SST and SIE). The sense of the response of the SO climate to AAMA in models is broadly consistent across studies (e.g. Stouffer et al., 2006; Aiken and England 2008; Bintanja et al., 2013 and 2015; Swart and Fyfe 2013; Rye et al., 2014 and 2020; Hansen et al., 2016; Pauling et al., 2016; Bronselaer e t al., 2018; Park and Latif 2018; Merino et al., 2018; Golledge et al., 2019). In addition, the work of Bronselaer et al., 2018, Golledge et al., 2019; Schloesser et al., 2019 and Mackie et al., (2020) suggest that increasing Antarctic melt anomaly drives global surface cooling, with the potential to significantly modify future projections.

Here we quantify and explore the mechanisms involved in such a response by utilising the Goddard Institute for Space Studies Earth System Model, denoted GISS-E2.1-G in the CMIP6 archive (Kelley et al., 2020). The modelling framework and pre-industrial climatological state of the coupled model is described in Kelley et al, (2020) and Miller et al (2020) - see also Supplementary Material (A) for more detail. In our first experiment, we make a step change in glacial meltwater anomalies imposed around Antarctica. To provide a reference point we also perform an experiment with an imposed step changes in atmospheric GHG concentrations enabling us to compare the pattern, timing and amplitude of the responses.

We use a range (500 to 30000 Gt/yr) of step-function perturbation experiments motivated by estimates of GHG driven melt rates by 2100 (Fig. 1e). The combined estimates of glacial melt from the Antarctic cryosphere (IMBIE 2018, Paolo 2015 and Shepherd et al 2010) suggest an additional glacial melt water flux into the Southern Ocean and Antarctic Subpolar Seas of between 500-750 Gt/yr over the last decade. Furthermore, future scenarios suggest a range from 800 Gt/yr to 25000 Gt/yr (32000 Gt/yr = 1Sv) by 2100 (e.g. Golledge et al., 2019; DeConto and Pollard, 2016).

Ensembles are employed to average out internal variability and are spawned by initiating experiments at 20-year intervals from a long control run; the number of ensembles used is discussed in the supplementary material. Meltwater adds fresh, cold water (due to extraction of latent heat required to melt the ice) which is released uniformly in the upper 200 meters of the ocean water column in a spatially-uniform manner in line with existing iceberg melt areas (Schmidt et al., 2014), as indicated in Fig.1d. Perturbation experiments are run for at least 30 years. Extended 100 year experiments are run for 2x CO_2 and 6000 Gt/yr perturbations (see Supp. Mat. For further details).

The response of the model to a range in meltwater forcing is shown in figure 2. To put the forcing magnitudes in context, by the end of this century GHG concentration might be in the range of 450-950 ppm according to the recently developed Shared Socioeconomic Pathways (SSPs), with warming in the range of 1.5-4.9°C (e.g. O'Neill et al 2016). The introduction of Antarctic melt anomalies drives a surface cooling ranging from 0.2 to 1.1 ºC over 30 years after an abrupt increase in AAMA forcing ranging from 500 to 30000 Gt/yr

(~0.015 to ~1 Sv). The surface temperature response is driven by surface cooling in the Southern Ocean further enhanced by a decline in global greenhouse capacity (the difference between longwave radiation emitted from the surface and that emitted at the top of the atmosphere) due primarily to a decline in atmospheric water vapour concentration. Of secondary importance for the higher AAMA input is an increase in (reflected) outgoing short-wave radiation, primarily associated with an increase in Southern Ocean sea ice extent.

Consistent with Schloesser et al., (2019) the response to increasing melt rates is sub-linear: weaker melt rates are found to drive a relatively larger magnitude surface cooling, whereas the model response ‘levels off’ with stronger melt rates (Figs. 2h, 2i). The response to increasing melt rates is found to stabilise for forcings above 10000 Gt/yr. The non-linear response and ultimate stabilization appear to be associated with the limitation on sea ice growth as AAMA increases. The first 4000 Gt y^{-1} increases Southern Hemisphere sea ice extent by about $5x10^6$ km^2, while the next 26000 Gt y^{-1} increases sea ice extent only by the same amount (Fig. 2a), and it is the cooling induced by sea ice that ultimately drives further reductions in water vapor (Fig. 2f) and greenhouse capacity (Fig. 2g), in an interactive feedback. Note that while the sea ice increase also leads to higher planetary albedo (Fig. 2d) and reduced shortwave forcing (Fig. 2e), these changes are only apparent at the greater AAMA input, and have a smaller effect on net radiation than does the reduced greenhouse capacity (Fig. 2c). The non-linear response may also be associated with limits to the suppression of Antarctic deep water formation (Li et al., 2020).

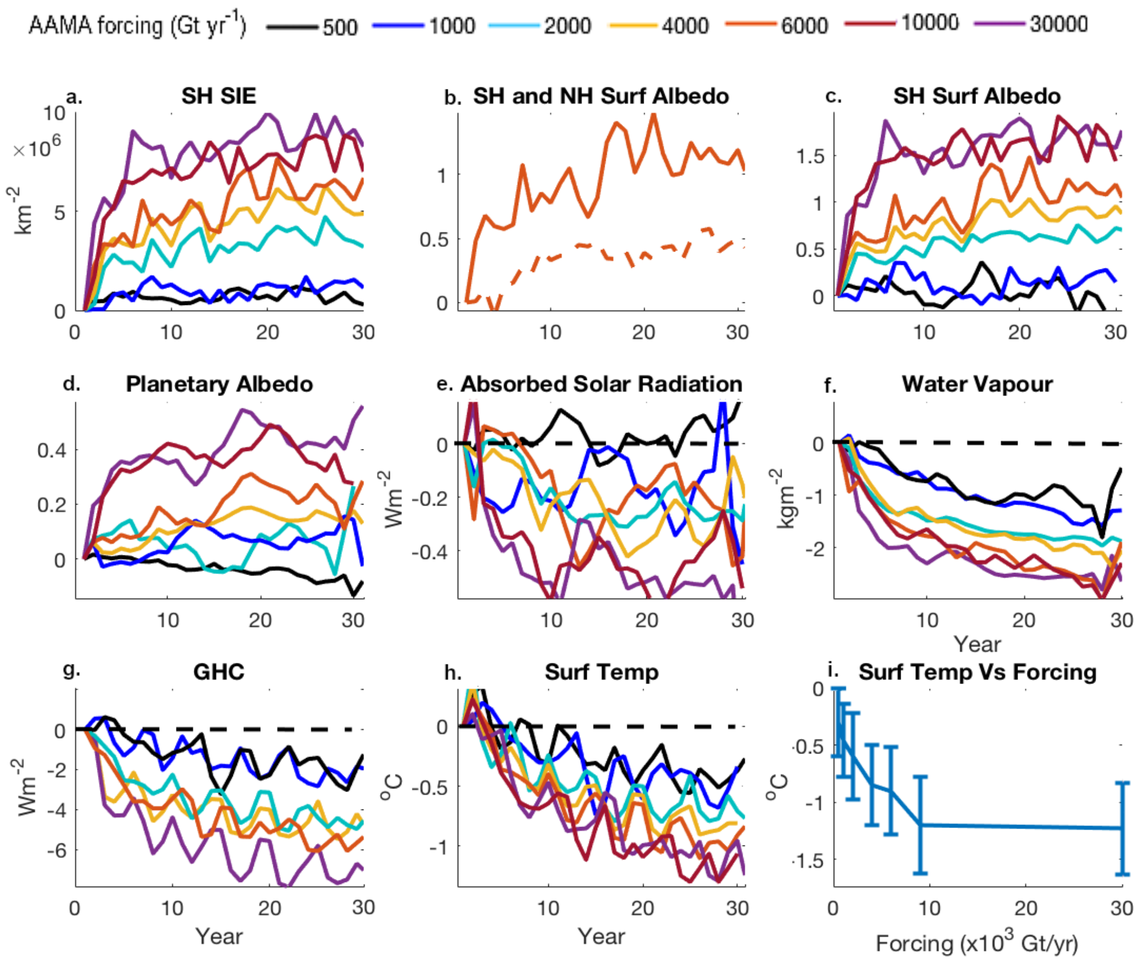

Figure 2| Response of GISS-2.1-G to a range in abrupt AAMA forcing's for key variables expressed as Climate Response Functions. Black lines: 500 Gt/yr, dark blue: 1000 Gt/yr, light blue: 2000 Gt/yr, yellow: 4000 Gt/yr, orange: 6000 Gt/yr, red: 10000 Gt/yr, purple: 30000 Gt/yr. a. Southern Hemisphere Sea Ice Extent. b. Southern Hemisphere (full line) and Northern Hemisphere (dashed line) surface albedo for 6000 Gt/yr. c. Southern Hemisphere Surface Albedo. d. Planetary Albedo (5-year smooth). e. Absorbed Solar Radiation (5-year smooth). f. Water Vapour (5-year smooth). g. Green House Capacity. h. Surface Temperature. i. Change in surface temperature after 30 years against abrupt AAMA forcing amount.

In Figures 3 and 4 we present key climate change indicators after 30 years of GHG and AAMA forcing (the plateau region in the CRF time series shown in Fig. 2) in our coupled model. We compare the 1.5xCO2 response, roughly corresponding to present day GHG forcing, to that of 1000 Gt/yr and 6000 Gt/yr, after 30 and 100 years. The former being a plausible current rate of melting and the latter more appropriate to the end of this century. In figure 3 we see the familiar global warming patterns in response to GHGs and the cooling patterns from AAMA. They are similar to mirror-images, except that the GHG response is largest over northern high-latitudes whereas the AAMA is largest in the south. The area weighted correlation of surface temperature anomalies driven by GHG and AAMA is around -0.4. The 6000 Gt/yr is somewhat larger than the 1.5xCO_2 response. Note that the interior ocean uniformly cools under AAMA forcing except around Antarctica, which warms over the whole water column and is associated with a weakening of Antarctic Bottom Water production.

In Figure 4 we map out anomalies in sea ice, planetary albedo, absorbed shortwave radiation, water vapour, and GHC. In the warming climate, sea ice reduction is larger in the Northern Hemisphere associated with its greater climatological extent, while in the AAMA experiments it increases primarily in the Southern Hemisphere due to the cold freshwater input. Absorbed shortwave radiation is affected locally by the sea ice changes, but with this magnitude of AAMA input its impact is minimal, due to the high latitudes and season of maximum sea ice growth. GHC and water vapour changes maximize in the tropics in both cases, even though the initial CO_2 forcing is global while the AAMA input is at high southern latitudes.

In Figure 5 we show the changes in the Ocean Heat Transport (OHT) and Meridional Overturning Circulation (MOC) for the global ocean. The difference in the response in OHT highlights the opposing characteristics of the forcing's (Fig. 5a,c). The GHG forcing case is associated with an increase in ocean heat transport in the Southern Hemisphere and decrease in the Northern Hemisphere; the AAMA response apposes this. With increased GHG the MOC decreases, associated with increased freshening and warming (Fig. 5d). The AAMA response, in contrast, has a very similar spatial signature to that induced by GHGs, but with the sign flipped (Fig. 5d,f), and for the opposite reasons. Associated northward ocean heat transports thus decrease in the North Atlantic with GHG increase (Fig. 5b), and increase with AAMA, creating opposing temperature patterns in the western North Atlantic (Figs. 3a,c).

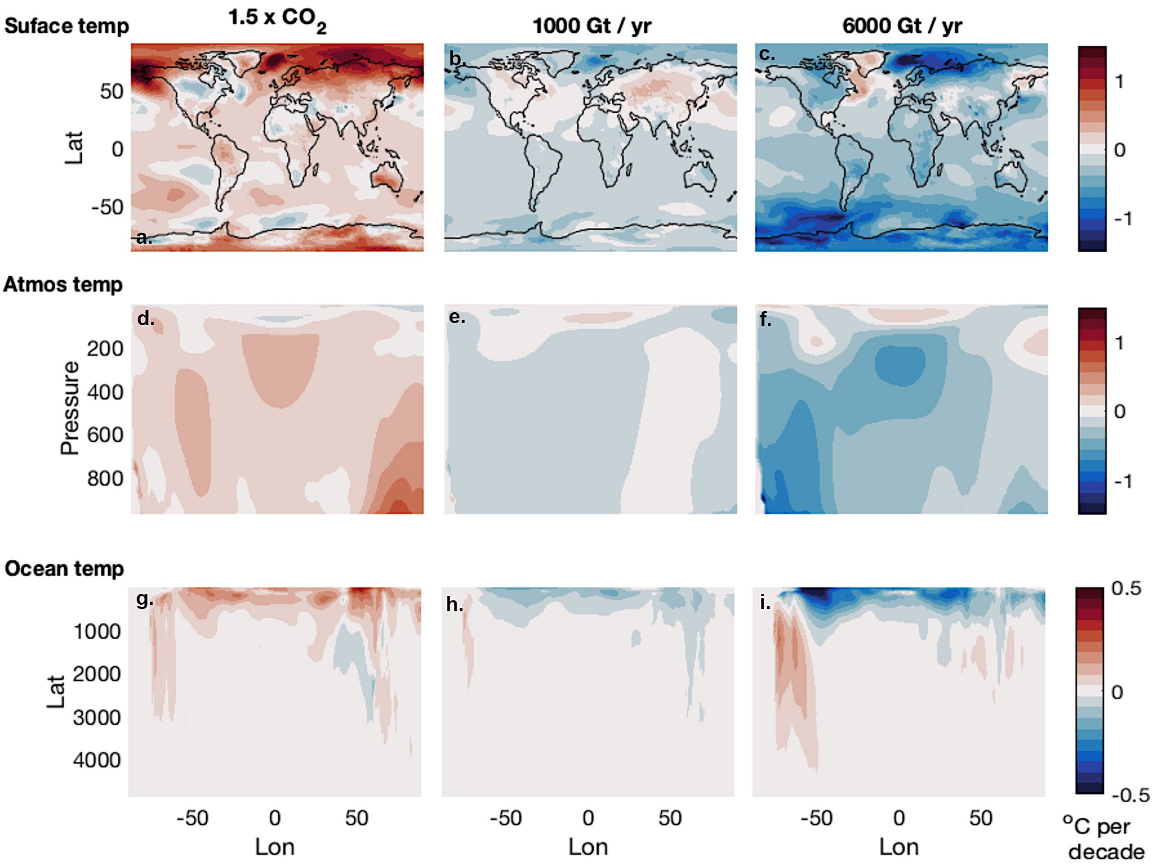

Figure 3 | Maps and zonal-mean sections of temperature trends in the atmosphere and ocean in response to GHG and AAMA forcing. Fields are averaged over 30 years for (left) 1.5 CO_2 (middle) 1000 Gt/yr and (right) 6000 Gt/yr of AAMA. The temperature scale for each row is the same and shown on the rhs.

Efficacy of Antarctic Glacial Melt forcing relative to other drivers

	2xCO2	1.5xCO2	500 Gt	1k Gt	2k Gt	4k Gt	6k Gt	10k Gt	30k Gt
GST Trend (K/yr) 0-30 yr	0.06 ±0.02	0.04 ±0.01	-0.01 ±0.01	-0.02 ±0.01	-0.02 ±0.01	-0.03 ±0.01	-0.04 ±0.02	-0.04 ±0.02	-0.04 ±0.02
ΔGST (K) avg yrs 20-30	1.50 ±0.31	1.08 ±0.28	-0.3 ±0.30	-0.46 ±0.32	-0.6 ±0.38	-0.85 ±0.35	-0.9 ±0.38	-1.1 ±0.42	-1.2 ±0.40
ΔGST (K) av 80-100 yr	1.60 ±0.31	1.20 ±0.32					-1.28 ±0.42		
α	-1.58 ±0.50	-2.00 ±0.50	-1.50 ±0.50	-1.70 ±0.50	-1.48 ±0.50	-1.70 ±0.50	-1.34 ±0.50	-1.32 ±0.50	-1.33 ±0.50
Eα		0.87 ±0.30	1.06 ±0.30	0.95 ±0.30	1.07 ±0.30	0.92 ±0.30	1.17 ±0.30	1.2 ±0.30	1.18 ±0.30

Table 1. Radiative forcing and efficacy of AAMA and CO_2 forcing | Columns from left to right show model results for abrupt increases of 2x and 1.5x CO_2, together with 500, 1000, 2000, 4000, 6000, 10000 and 30000 Gt/yr AAMA. Rows from top to bottom show: the change in global surface temperature (GST) averaged over 30 years (following an abrupt change in forcing); global surface temperature (GST) anomaly averaged between 25-30 years; global surface temperature (GST) anomaly averaged between 80-100 years (these numbers are provided for 1.5 x CO_2 and 6000 Gt/yr only for comparison to Richardson et al., (2019)); the feedback parameter, α; the efficacy E_α estimated from α, as described by Richardson et al., 2019 and in Supplementary Materials.

The global surface air temperature changes in the different GHG and AAMA experiments are shown in Table. 1. Beginning with the surface air temperature change, the cooling averaged between years 20-30 for 500 Gt/yr AAMA is about 25-30% of the warming induced by current CO_2 levels over that period. To reach the instantaneous doubled CO_2 value of 1.5ºC in that short period would require an input of much greater than 30,000 Gt/yr. This would seem to be the case even for longer integrations, considering the 6K Gt/yr result after 80-100 years.

We compare the ability of glacial meltwater input to change the global mean temperature relative to that of CO_2; this ability relative to that of doubled CO_2 is termed the 'efficacy', defined here in terms of feedback factors:

$$E_\alpha = \frac{\alpha_{CO_2}}{\alpha_f}$$

where α_{CO2} is the feedback associated with CO_2 and α_f the feedback associated with the forcing in question.

The feedback factor is calculated using linear regression of the global mean top of the atmosphere radiative flux change against surface air temperature. A higher feedback parameter is associated with a smaller climate sensitivity, as less surface air temperature change is required to restore the climate system to equilibrium. The feedback factors for the different experiments are shown in Table 1. We see that the feedback factor for glacial melt is comparable to, but smaller than for increased CO_2 for all AAMA forcings. Note also that the feedback parameter decreases with increasing AAMA rates. This reduction is likely associated with the high latitude of the glacial meltwater input which is distant from tropical atmospheric water vapor reservoirs. The increased climate sensitivity which the reduced value implies may be associated with the high latitude amplification of temperature changes.

The efficacy based on the feedback parameter at small glacial inputs is slightly greater than for the current CO_2 values, and increases further at inputs greater than 1k Gt/yr. This suggests that the feedbacks associated with the response to AAMA forcing are similar to the feedbacks associated with CO_2.

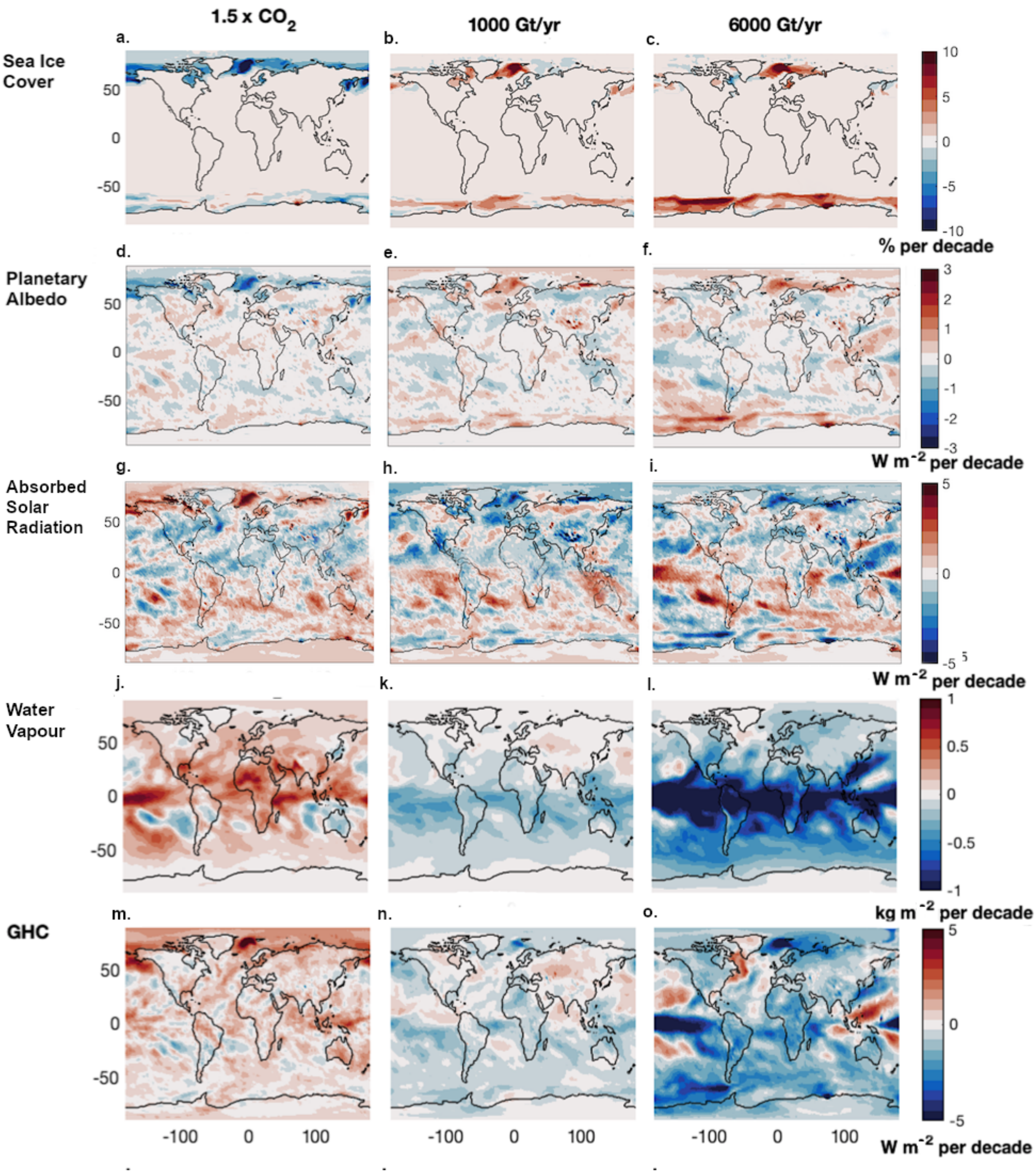

Figure 4 | Maps of climate trends highlighting mechanisms between GHG, AAMA and warming, cooling. Fields are averaged over 30 years for (left) 1.5 CO2 (middle) 1000 Gt/yr and (right) 6000 Gt/yr of AAMA. Row 1 shows decadal trends in Sea Ice cover, Row 2 trends in Planetary Albedo, Row 3 trends in the Absorbed Solar Radiation, Row 4, trends Water Vapour and Row 5 trends in Green House Capacity. The scales for each row are the same and shown on the rhs.

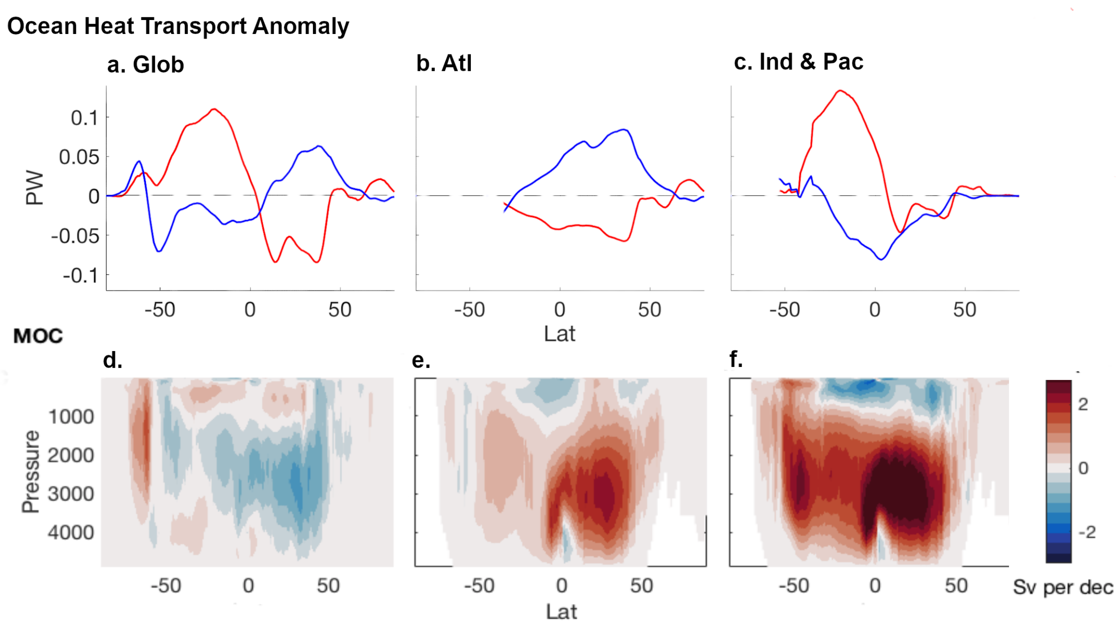

Figure 5 | Ocean heat transport and overturning. a-c. Zonal-mean northward ocean heat transport anomaly, red lines: for 1.5xCO_2. Blue lines: for 6000 Gt/yr AAMA forcing. Anomaly is averaged over years 20-30 following an abrupt change in forcing. a. Global average values. b. Atlantic. c. Indian + Pacific. d-f. Trend in meridional overturning function. Fields are averaged over 30 years for (left) 1.5xCO_2 (middle) 1000 Gt/yr and (right) 6000 Gt/yr of AAMA.

Various approaches to determining efficacy have been explored in our study, as presented in Supplementary Material (B), and all yield broadly similar results. It is important to realize that the process by which AAMA influences global climate differs from that of other forcings in that it is initially very much local, and the local cooling only gradually extends its effect to the global domain through (mainly) water vapor feedbacks. Thus, a standard approach to determining efficacy, in which the instantaneous or effective radiative forcing is compared with the ultimate temperature response, is less useful here. Instead of using instantaneous forcing, in the supplementary materials we use the average forcing over the first 20-30 years; this produces results identical to the feedback factor approach described above.

Discussion and Conclusions

We have found that plausible Antarctic glacial melt rates of a few 1000 Gt/yr can elicit a cooling response that significantly ameliorates expected GHG warming – see Figs. 2h&i. Making use of linear convolution theory and assuming a relationship between global surface temperature anomaly and AAMA as suggested by DeConto and Pollard, (2016) or Golledge et al., (2019), we expect that by mid-century cooling by AAMA forcing may reduce global warming by 10 to 30% (see the discussion in Supplementary Materials (C)). This is broadly consistent with the direct scenario studies of Bronselaer et al., 2018 and Golledge et al., 2019. The non-linearity of the response to forcing amplitude, clearly exposed by our CRF approach and our mechanistic exploration, enables us to rationalise these results. We conclude that if current trends in Southern Ocean continue, along with associated surface freshening, cooling and sea ice stabilisation/expansion, AAMA is likely to constitute an important player in climate projections. In many respects the associated temperature change, induced globally and in all three-dimensions, is similar but approximately opposite to that associated with GHGs. This includes temperature changes of both signs associated with altered heat transports by AMOC changes, increased into the North Atlantic with AAMA, decreased with increasing CO2. If GHG levels follow an extreme scenario, however, our results suggest that the cooling effect of plausible AAMA melt rates will be overwhelmed by the end of the century.

The mechanism that drives a global response to localised high-latitude freshwater input is of great importance and interest. The forcing associated with glacial meltwater input is focused on high latitudes, rather than having the immediate global shortwave reach of solar and aerosol forcing. However, it subsequently acts in a broadly similar way to globally distributed forcings, initiating climate feedbacks and producing temperature changes with similar efficacy, temperature changes which extend globally, including in the tropics. This ability of high latitude aspects of the climate system to initiate such global responses if sustained over time is reported in, for example, Rind et al. (1995). Nevertheless, high latitude forcing of global climate is often discounted, based on the observed inability of volcanoes poleward of 50° latitude to generate a noticeable global temperature change.

Finally, our perturbation experiments are unable to represent feedbacks between AAMA and the climate. Assuming that the rate of AAMA is a function of global surface temperature, increasing AAMA will reduce surface temperatures and hence, presumably, reduce AAMA production, thus acting as a negative feedback. However, Bronselaer et al., (2018), argues that AAMA drives an increase in heat content on the Antarctic shelf and therefore a positive feedback on AAMA. Finally, Zelinka et al., 2020, argue that models which have large SO cloud feedbacks have a particularly high ECS. Such models may exhibit a different efficacy for AAMA. Experiments of the kind described here need to be carried out with a range of coupled models to document the robustness of the climate response to AAMA.

References

Abernathey, R.P., Cerovecki, I., Holland, P.R., Newsom, E., Mazloff, M. and Talley, L.D., 2016. Water-mass transformation by sea ice in the upper branch of the Southern Ocean overturning. *Nature Geoscience*, *9*(8), pp.596-601.

Adusumilli, S., Fricker, H.A., Medley, B., Padman, L. and Siegfried, M.R., 2020. Interannual variations in meltwater input to the Southern Ocean from Antarctic ice shelves. *Nature Geoscience*, *13*(9), pp.616-620.

Aiken, C.M. and England, M.H., 2008. Sensitivity of the present-day climate to freshwater forcing associated with Antarctic sea ice loss. *Journal of climate*, *21*(15), pp.3936-3946.

Barthélemy, A., Goosse, H., Mathiot, P. and Fichefet, T., 2012. Inclusion of a katabatic wind correction in a coarse-resolution global coupled climate model. *Ocean Modelling*, *48*, 45-54.

Bintanja, R., Van Oldenborgh, G.J., Drijfhout, S.S., Wouters, B. and Katsman, C.A., 2013. Important role for ocean warming and increased ice-shelf melt in Antarctic sea-ice expansion. *Nature Geoscience*, *6*(5), pp.376-379.

Bintanja, R., Van Oldenborgh, G.J. and Katsman, C.A., 2015. The effect of increased fresh water from Antarctic ice shelves on future trends in Antarctic sea ice. *Annals of Glaciology*, *56*(69), pp.120-126.

Bronselaer, B., Winton, M., Griffies, S.M., Hurlin, W.J., Rodgers, K.B., Sergienko, O.V., Stouffer, R.J. and Russell, J.L., 2018. Change in future climate due to Antarctic meltwater. *Nature*, *564*(7734), pp.53-58.

DeConto, R.M. and Pollard, D., 2016. Contribution of Antarctica to past and future sea-level rise. *Nature*, *531*(7596), pp.591-597.

Doddridge, E.W., Marshall, J., Song, H., Campin, J.M., Kelley, M. and Nazarenko, L., 2019. Eddy compensation dampens Southern Ocean sea surface temperature response to westerly wind trends. *Geophysical Research Letters*, *46*(8), pp.4365-4377.

England, M., Polvani, L. and Sun, L., 2018. Contrasting the Antarctic and Arctic atmospheric responses to projected sea ice loss in the late twenty-first century. *Journal of Climate*, *31*(16), pp.6353-6370.

England, M.H., 1992. On the formation of Antarctic Intermediate and Bottom Water in Ocean general circulation models. *Journal of Physical Oceanography*, *22*(8), pp.918-926.

Golledge, N.R., Keller, E.D., Gomez, N., Naughten, K.A., Bernales, J., Trusel, L.D. and Edwards, T.L., 2019. Global environmental consequences of twenty-first-century ice-sheet melt. *Nature*, *566*(7742), pp.65-72.

Hansen, J., Sato, M., Hearty, P., Ruedy, R., Kelley, M., Masson-Delmotte, V., Russell, G., Tselioudis, G., Cao, J., Rignot, E. and Velicogna, I., 2015. Ice melt, sea level rise and superstorms: evidence from paleoclimate data, climate modeling, and modern observations that 2° C global warming is highly dangerous. *Atmospheric Chemistry & Physics Discussions*, *15*(14).

Haumann, F.A., Gruber, N., Münnich, M., Frenger, I. and Kern, S., 2016. Sea-ice transport driving Southern Ocean salinity and its recent trends. *Nature*, *537*(7618), pp.89-92.

Holland, P.R., Bracegirdle, T.J., Dutrieux, P., Jenkins, A. and Steig, E.J., 2019. West Antarctic ice loss influenced by internal climate variability and anthropogenic forcing. *Nature Geoscience*, *12*(9), pp.718-724.

IMBIE 2018, Shepherd, A., Ivins, E., Rignot, E., Smith, B., Van Den Broeke, M., Velicogna, I., et al. (2018). Mass balance of the Antarctic Ice Sheet from 1992 to 2017. *Nature*, *558*, pp.219-222.

Li, G., Cheng, L., Zhu, J., Trenberth, K.E., Mann, M.E. and Abraham, J.P., 2020. Increasing ocean stratification over the past half-century. *Nature Climate Change*, pp.1-8.

Jenkins, A., Dutrieux, P., Jacobs, S., Steig, E.J., Gudmundsson, G.H., Smith, J. and Heywood, K.J., 2016. Decadal ocean forcing and Antarctic ice sheet response: Lessons from the Amundsen Sea. *Oceanography*, *29*(4), pp.106-117.

Kelley, M., Schmidt, G.A., Nazarenko, L.S., Bauer, S.E., Ruedy, R., Russell, G.L., Ackerman, A.S., Aleinov, I., Bauer, M., Bleck, R. and Canuto, V., 2020. GISS‐E2. 1: Configurations and Climatology. *Journal of Advances in Modeling Earth Systems*, *12*(8), p.e2019MS002025

Kostov, Y., Marshall, J., Hausmann, U., Armour, K.C., Ferreira, D. and Holland, M.M., 2017. Fast and slow responses of Southern Ocean sea surface temperature to SAM in coupled climate models. *Climate Dynamics*, *48*(5-6), pp.1595-1609.

Kostov, Y., Ferreira, D., Armour, K.C., and Marshall, J., 2018: Contributions of Greenhouse Gas Forcing and the Southern Annular Mode to Historical Southern Ocean Surface Temperature Trends. *Geophysical Research Letters*, vol. 45. doi = 10.1002/2017GL074964

Mackie, S., Smith, I.J., Ridley, J.K., Stevens, D.P. and Langhorne, P.J., 2020. Climate response to increasing Antarctic iceberg and ice shelf melt. *Journal of Climate*, *33*(20), pp.8917-8938.

Marshall, J., Armour, K.C., Scott, J.R., Kostov, Y., Hausmann, U., Ferreira, D., Shepherd, T.G. and Bitz, C.M., 2014. The ocean's role in polar climate change: asymmetric Arctic and Antarctic responses to greenhouse gas and ozone forcing. *Philosophical Transactions of the Royal Society A: Mathematical, Physical and Engineering Sciences*, *372*(2019), p.20130040.

Marshall, J., Scott, J.R., Romanou, A., Kelley, M. and Leboissetier, A., 2017. The dependence of the ocean’s MOC on mesoscale eddy diffusivities: A model study. *Ocean Modelling*, *111*, pp.1-8.

Morales Maqueda, M.A., Willmott, A.J. and Biggs, N.R.T., 2004. Polynya dynamics: A review of observations and modeling. *Reviews of Geophysics*, *42*(1).

Merino, N., Jourdain, N.C., Le Sommer, J., Goosse, H., Mathiot, P. and Durand, G., 2018. Impact of increasing antarctic glacial freshwater release on regional sea-ice cover in the Southern Ocean. *Ocean Modelling*, *121*, pp.76-89.

Miller, R.L., Bauer, S.E., Tsigaridis, K., Faluvegi, G., Kelley, M., Lo, K.K., Nazarenko, L., Schmidt, G.A. and Wu, J., 2020. Historical (1850–2014) aerosol evolution and role on climate forcing using the GISS ModelE2. 1 contribution to CMIP6. *Journal of Advances in Modeling Earth Systems*, *12*(8), p.e2019MS001978.

Moorman, R., Morrison, A.K. and McC. Hogg, A., 2020. Thermal Responses to Antarctic Ice Shelf Melt in an Eddy-Rich Global Ocean–Sea Ice Model. *Journal of Climate*, *33*(15), pp.6599-6620.

Nakayama, Y., Timmermann, R., Schröder, M. and Hellmer, H.H., 2014. On the difficulty of modeling Circumpolar Deep Water intrusions onto the Amundsen Sea continental shelf. *Ocean Modelling*, *84*, pp.26-34.

O'Neill, B.C., Tebaldi, C., Van Vuuren, D.P., Eyring, V., Friedlingstein, P., Hurtt, G., Knutti, R., Kriegler, E., Lamarque, J.F., Lowe, J. and Meehl, G.A., 2016. The scenario model intercomparison project (ScenarioMIP) for CMIP6.

Paolo, F.S., Fricker, H.A. and Padman, L., 2015. Volume loss from Antarctic ice shelves is accelerating. *Science*, *348*(6232), pp.327-331.

Parkinson, C.L., 2019. A 40-y record reveals gradual Antarctic sea ice increases followed by decreases at rates far exceeding the rates seen in the Arctic. *Proceedings of the National Academy of Sciences*, *116*(29), pp.14414-14423.

Park, W., and Latif, M. 2018. Ensemble global warming simulations with idealized Antarctic meltwater input. Climate Dynamics, 52, 3223–3239.

Pauling, A.G., Bitz, C.M., Smith, I.J. and Langhorne, P.J., 2016. The response of the Southern Ocean and Antarctic sea ice to freshwater from ice shelves in an Earth system model. *Journal of Climate*, *29*(5), pp.1655-1672.

Rind, D., Healy, R., Parkinson, C. and Martinson, D., 1995. The role of sea ice in 2× CO_2 climate model sensitivity. Part I: The total influence of sea ice thickness and extent. *Journal of Climate*, *8*(3), pp.449-463.

Richardson, T.B., Forster, P.M., Smith, C.J., Maycock, A.C., Wood, T., Andrews, T., Boucher, O., Faluvegi, G., Fläschner, D., Hodnebrog, Ø. and Kasoar, M., 2019. Efficacy of climate forcings in PDRMIP models. *Journal of Geophysical Research: Atmospheres*, *124*(23), pp.12824-12844.

Russell, J.L., Kamenkovich, I., Bitz, C., Ferrari, R., Gille, S.T., Goodman, P.J., Hallberg, R., Johnson, K., Khazmutdinova, K., Marinov, I. and Mazloff, M., 2018. Metrics for the evaluation of the Southern Ocean in coupled climate models and earth system models. *Journal of Geophysical Research: Oceans*, *123*(5), pp.3120-3143.

Rye, C.D., Garabato, A.C.N., Holland, P.R., Meredith, M.P., Nurser, A.G., Hughes, C.W., Coward, A.C. and Webb, D.J., 2014. Rapid sea-level rise along the Antarctic margins in response to increased glacial discharge. *Nature Geoscience*, *7*(10), pp.732-735.

Rye, C.D., Marshall, J., Kelley, M., Russell, G., Nazarenko, L.S., Kostov, Y., Schmidt, G.A. and Hansen, J., 2020. Antarctic Glacial Melt as a Driver of Recent Southern Ocean Climate Trends. *Geophysical Research Letters*, *47*(11), p.e2019GL086892.

Sasgen, I., Wouters, B., Gardner, A.S., King, M.D., Tedesco, M., Landerer, F.W., Dahle, C., Save, H. and Fettweis, X., 2020. Return to rapid ice loss in Greenland and record loss in 2019 detected by the GRACE-FO satellites. *Communications Earth & Environment*, *1*(1), pp.1-8.

Schloesser, F., Friedrich, T., Timmermann, A., DeConto, R.M. and Pollard, D., 2019. Antarctic iceberg impacts on future Southern Hemisphere climate. *Nature Climate Change*, *9*(9), pp.672-677.

Schmidt, G.A., Kelley, M., Nazarenko, L., Ruedy, R., Russell, G.L., Aleinov, I., Bauer, M., Bauer, S.E., Bhat, M.K., Bleck, R., Canuto, V. et al., 2014. Configuration and assessment of the GISS ModelE2 contributions to the CMIP5 archive. *Journal of Advances in Modeling Earth Systems*, *6*(1), pp.141-184.

Sen Gupta, A., Santoso, A., Taschetto, A.S., Ummenhofer, C.C., Trevena, J. and England, M.H., 2009. Projected changes to the Southern Hemisphere ocean and sea ice in the IPCC AR4 climate models. *Journal of Climate*, *22*(11), pp.3047-3078.

Seviour, W.J., Gnanadesikan, A., Waugh, D. and Pradal, M.A., 2017. Transient response of the Southern Ocean to changing ozone: Regional responses and physical mechanisms. *Journal of Climate*, *30*(7), pp.2463-2480.

Seroussi, H., Nakayama, Y., Larour, E., Menemenlis, D., Morlighem, M., Rignot, E. and Khazendar, A., 2017. Continued retreat of Thwaites Glacier, West Antarctica, controlled by bed topography and ocean circulation. *Geophysical Research Letters*, *44*(12), pp.6191-6199.

Shepherd, A., Wingham, D., Wallis, D., Giles, K., Laxon, S. and Sundal, A.V., 2010. Recent loss of floating ice and the consequent sea level contribution. *Geophysical Research Letters*, *37*(13).

Stouffer, R.J., Seidov, D. and Haupt, B.J., 2007. Climate response to external sources of freshwater: North Atlantic versus the Southern Ocean. *Journal of Climate*, *20*(3), pp.436-448.

Swart, N.C. and Fyfe, J.C., 2013. The influence of recent Antarctic ice sheet retreat on simulated sea ice area trends. *Geophysical Research Letters*, *40*(16), pp.4328-4332.

Tollefson, J., 2020. How hot will Earth get by 2100? *Nature*, *580*(7804), pp.443-445.

Wang, C., Zhang, L., Lee, S.K., Wu, L. and Mechoso, C.R., 2014. A global perspective on CMIP5 climate model biases. *Nature Climate Change*, *4*(3), pp.201-205.

Zelinka, M.D., Myers, T.A., McCoy, D.T., Po‐Chedley, S., Caldwell, P.M., Ceppi, P., Klein, S.A. and Taylor, K.E., 2020. Causes of higher climate sensitivity in CMIP6 models. *Geophysical Research Letters*, *47*(1), p.e2019GL085782.

Zhang, J., 2014. Modeling the impact of wind intensification on Antarctic sea ice volume. *Journal of Climate*, *27*(1), pp.202-214.

Supplementary Material:

(A) Modelling Framework and Experiment design

1. GISS Model E

We use the NASA Goddard Institute for Space Studies (GISS) earth system model, ModelE. This configuration integrates Atmosphere, Ocean, Land and Cryosphere components (Schmidt et al., 2006; Schmidt et al., 2014, Kelley et al, 2020). The Atmosphere comprises 40 vertical levels with a horizontal resolution of 2 x 2.5 degrees. It uses an Arakawa-B grid and a sigma vertical coordinate extending to 0.1 hPa. The Ocean has 40 vertical levels with 1 degree horizontal resolution on a modified Arakawa C-grid scheme. Vertical mixing uses the KPP scheme (Large et al., 1996). Mesoscale eddies and isopycnal diffusion are parameterized by the Gent and McWilliams (1996) scheme with variable coefficients (Visbeck et al., 1997; Griffies 1998) as described in Marshall et al, 2017 and Kelley et al, 2020. The ModelE sea ice model consists of two mass layers and four thermal layers. Salinity and tracers are calculated on mass layers. Sea ice dynamics utilizes the viscous-plastic formulation of Zhang and Rothrock (2000) and the brine-pocket thermodynamics of Bitz and Lipscomb (1999).

The ice-sheet module is coupled to the ocean through an idealized representation of melting icebergs, referred to as the implicit ice-berg array. The standard ice-sheet model is not dynamic and acts to maintain constant ice-sheet mass; excess precipitation onto the Antarctic continent is collected into the implicit ice-berg array and released into the ocean over a 10-year period. The iceberg array distributes meltwater evenly as defined by the mask shown in figure 1d. The standard ModelE iceberg mask follows observations of iceberg calving (Tournadre et al., 2016). Meltwater is distributed evenly in the upper 200 meters. The iceberg array has climatological annual flux of around 1800 Gt/yr, consistent with observations.

2. Climate Response Function (CRF) and ensemble technique

The use of CRFs to probe the response of climate to drivers is briefly reviewed in Marshall et al., 2014, together with the associated linear convolution theory. Here the CRFs shown in Figure 2 are estimated as area weighted global averages - unless stated as northern or southern hemisphere – and are also averaged across ensembles. The number of ensembles used varies between forcing levels: 10, 5, 3, 1, 1 and 1 for forcings of 500, 1000, 2000, 6000, 10000, 30000 Gt/yr respectively. The Green House Capacity (Figure 2g) is estimated as the difference between long wave radiation emitted from the surface and long wave emitted away from the earth at the top of the atmosphere. The Planetary Albedo, Absorbed Solar Radiation and Water Vapour (Figure 2d-f) are smoothed over a 5-year period to reduce noise from internal variability.

3. Limitations of modelling framework

There are known shortcomings associated with the representation of the Antarctic Subpolar Seas in relatively low-resolution coupled earth system models such as the one used here. These models poorly represent features such as the Antarctic slope front (Nakayama et al., 2014, Moorman et al., 2020) and surface winds, particularly the position of the zero wind line (e.g. Russell et al., 2018). They are also unable to represent many important features such as, polynyas (e.g. Maqueda 2004), katabatic winds (Barthelemy et al., 2012), and deep-water formation (England 1992). For example, high resolution, ocean-only modelling studies suggest that additional melt water may be more constrained to the coast then is found in lower resolution coupled models, and this is likely to impact the results.

Our conclusions crucially depend on the effect that glacial meltwater has on sea ice extent. However the mechanistic connection between the drivers of AAMA, AAMA and sea ice extent are not fully understood and are very challenging to represent in climate models.

The majority of AAMA over recent decades has been produced in the Bellingshausen /Amundsen Seas (Pacific Ocean Sector, e.g. Paolo et al. 2015). In this region warm circumpolar deep water is being drawn onto the shelf where it is able to access the underside of the ice shelves (Nakayama et al., 2014). The heat content of these shelf waters is observed to vary on decadal timescales in step with tropical variability (Jenkins 2016), but it is also suggested to be steadily warming associated with GHG forcing (Holland et al., 2019). Both of these types of variability are modulated by changes in the surface wind field which is also affected by anthropogenic forcings – notably stratospheric ozone depletion and CO_2 (Miller et al., 2006 and others). Further, the vulnerability of the Antarctic Ice Shelf to ocean melting is modulated by specific regional topography and ice shelf geometry that promote additional non-linearities in melt rate (e.g. Seroussi et al., 2017). Counter-intuitively sea ice extent has been observed to reduce in the Amundsen/Bellingshausen over recent decades (Parkinson 2019), precisely where model results suggest AAMA-induced sea ice increasing, suggesting that we may be misrepresenting AAMA transport, local changes in ocean conditions or local surface atmosphere conditions in our models. Many of the above processes and interactions are absent or poorly represented in the modelling framework and meltwater experiments discussed here.

Despite the above limitations, the coupled model employed here has a remarkably good climatology, particularly in the southern hemisphere, capturing the seasonal cycle of SST and sea-ice distribution: see Fig.1, Kelley et al, 2020 and Rye et al., 2020.

(B) Determination of Efficacies of climate forcings

In order to estimate the efficacy of AAMA forcing in driving global surface temperature change we estimate the response of the model in terms of radiative forcings and associate these forcings with their respective change in surface temperature. We first estimate the instantaneous radiative forcing at the TOA by averaging the radiative forcing anomaly at this level over the first 5 years. The radiative forcing anomaly from AAMA is largest in the first 3 years associated with sea ice growth; this anomaly tends to 0 as the climate adjusts.

The instantaneous radiative forcing at the top of the atmosphere resulting from 500 Gty/year glacial water input is of a similar magnitude (with reverse sign) to the current 1.5xCO2 increase, but even the largest meltwater input used only provides 2/3 the magnitude of radiative forcing of an instantaneous input of 2xCO_2. These values will provide one estimate of glacial meltwater efficacy.

We calculate an 'effective radiative forcing' by using linear regression of global mean TOA flux change against the global surface air temperature change relative to the baseline simulation for the first 20 years of the coupled simulations. This 'regression' effective radiative forcing is given by the intercept of the regression line where $\Delta T = 0$ (Gregory, 2004). The approach allows stratospheric, tropospheric, and land surface feedback mechanisms to operate. As shown in the Table, the values for the glacial meltwater inputs are somewhat lower than the current CO2 increase and this is true for even the largest meltwater input. We will use these results to calculate another set of efficacy values.

An additional 'effective' radiative forcing assessment has been used in studies (e.g., Richardson et al. 2019) to isolate the initial radiative forcing from the system response, by keeping the SSTs and sea ice fixed to minimize water vapor and cloud feedback. This cannot be done in the case of glacial melt, since the only way it influences the system initially is by changing SSTs and sea ice distributions.

A concern with the instantaneous radiative forcing and effective radiative forcing calculations is that these diagnostics are designed to assess the impact of an instantaneous change in atmospheric composition such as an increase in CO_2 or sulphate aerosols. In these cases the temperature anomaly at t=0 is 0 and the radiative anomaly is large, as time progresses the temperature anomaly increases as the radiative anomaly tends to 0. However, in the case of meltwater forcing at t=0 both the temperature anomaly and radiative anomaly are close to 0, AAMA forcing drives an anomaly in the radiative forcing that reaches a maximum in the first 5 years and then trends to 0 as the temperature anomaly tends to a new equilibrium. These differences in the characteristic response suggest that the instantaneous radiative forcing and effective radiative forcing may not be well posed to describe the response of the system to a forcing such as Antarctic melt water that has an impact on the surface temperature by initiating an increase in sea ice and driving the water vapour feedback. Therefore, an additional approach to estimating an effective radiative forcing is taken. The surface temperature anomaly averaged over the last 5 years following an abrupt increase in melt water forcing is multiplied by the slope of the linear regression of global mean TOA flux change against the global surface air temperature change relative. The slope of this line is referred to as alpha, the climate feedback parameter. This additional estimate of forcing is referred to here as the effective equivalent forcing (F_{eq}).

Then we determine an “efficacy”, which is defined as the ability of that climate forcing to generate a surface air temperature change compared to that for $2xCO_2$. The change of climate due to glacial meltwater input into the SO is a different type of forcing than others generally considered. Nevertheless, we can still quantify the resultant radiative forcing and efficacy of its impact compared to that of other forcing agents. The results are set out in Table 1 and compared to that from various CO2 forcings. Surface air temperature changes and radiative forcings for 2xCO2 are first tabulated. Then shown are model responses to glacial meltwater input varying from 500 Gt/yr (approximately the current situation) to 30,0000 Gt/yr, as well as the values for 1.5xCO_2 chosen to approximately correspond to current levels of GHG forcing.

We can compute an efficacy by dividing the temperature response by the appropriate forcing or parameter, and normalizing that ratio with respect to the same ratio for doubled CO_2, i.e.,

$$E_f = \frac{\Delta T/F}{\Delta T_{2\times CO2}/F_{2\times CO2}},$$

where F is either the instantaneous forcing or the effective (regression) radiative forcing. Considering first the efficacy associated with the instantaneous radiative forcing, the smaller magnitudes of glacial meltwater input has somewhat reduced values compared to that of the current CO_2 level, while greater glacial input has somewhat larger values. The efficacy considering 'effective' radiative forcing is similar to current CO_2 levels for small meltwater input and becomes larger with magnitudes greater than 1k Gt/yr input.

	2xCO_2	**1.5xCO_2**	**500 Gt**	**1k Gt**	**2k Gt**	**4k Gt**	**6k Gt**	**10k Gt**	**30k Gt**
ΔGST (K/yr) over 30 yr	0.06 ±0.02	0.04 ±0.01	-0.02 ±0.01	-0.02 ±0.01	-0.02 ±0.01	-0.03 ±0.01	-0.04 ±0.02	-0.04 ±0.02	-0.04 ±0.02
ΔGST (K) 20-30 yrs	1.50 ±0.31	1.08 ±0.28	-0.3 ±0.30	-0.46 ±0.32	-0.6 ±0.38	-0.85 ±0.35	-1.1 ±0.38	-1.3 ±0.42	-1.3 ±0.40
ΔGST (K) 80-100 yrs	1.60 ±0.31	1.20 ±0.32					-1.28 ±0.42		
IRF TOA (Wm^{-2})	2.70 ±0.60	1.99 ±0.60	-0.6 ±0.60	-0.6 ±0.60	-1 ±0.60	-1.1 ±0.60	-1.25 ±0.60	-1.27 ±0.60	-1.4 ±0.60
ERF (Wm^{-2})	3.40 ±0.30	2.70 ±0.30	-0.9 ±0.30	-1 ±0.30	-1 ±0.30	-1 ±0.30	-1.5 ±0.30	-1.55 ±0.30	-1.6 ±0.30
EEF (Wm^{-2})	2.37 ±0.50	2.16 ±0.50	-0.69 ±0.50	-0.85 ±0.50	-0.88 ±0.50	-1.44 ±0.50	-1.47 ±0.50	-1.6 ±0.50	-1.7 ±0.50
α	-1.58 ±0.50	-2.00 ±0.50	-1.50 ±0.50	-1.70 ±0.50	-1.48 ±0.50	-1.70 ±0.50	-1.34 ±0.50	-1.32 ±0.50	-1.33 ±0.50
E_{IRF}	20-30yrs 80-100yrs	0.98 ±0.30 0.95 ±0.30	1.39 ±0.30, -	1.5 ±0.30, -	1.1 ±0.30, -	1.4 ±0.30, -	1.6 ±0.30 1.48 ±0.30	1.72 ±0.30, -	1.68 ±0.30, -
E_{ERF}	20-30yrs 80-100yrs	0.92 ±0.30 0.95 ±0.30	1.16 ±0.30 -	1.13 ±0.30, -	1.36 ±0.30, -	1.93 ±0.30, -	1.66 ±0.30, 1.51 ±0.30	1.76 ±0.30 -	1.85 ±0.30 -
E_{EEF}		0.81 ±0.5	1.06 ±0.5	0.93 ±0.50	1.2 ±0.50	0.93 ±0.50	1.18 ±0.50	1.19 ±0.50	1.2 ±0.50
E_{α}		0.87 ±0.30	1.06 ±0.30	0.95 ±0.30	1.07 ±0.30	0.92 ±0.30	1.17 ±0.30	1.2 ±0.30	1.18 ±0.30
Ratio of ERF 30/100 yrs		1.04					0.91		

Table 1. Radiative forcing and efficacy of AAMA and CO_2 forcing (Extended table) | Columns from left to right show model results for abrupt increases of 2x and 1.5xCO_2, as well as 500, 1000, 2000, 4000, 6000, 10000 and 30000 Gt/yr AAMA. Rows from top to bottom show the change in global surface temperature (GST) averaged over 30 years (following an abrupt change in forcing). The average global surface temperature (GST) anomaly averaged between 25-30 years. Then the average global surface temperature (GST) anomaly averaged between 80-100 years (these numbers are provided for 1.5 x CO_2 and 6000 Gt/yr only for comparison to Richardson et al., (2019)). Instantaneous radiation forcing at TOA (IRF TOA) averaged over the first 5 years, Effective Radiative Forcing (ERF), Effective Equivalent Forcing (EEF), the feedback parameter α, Efficacy estimated from Instantaneous Radiative

Forcing E_{IRF}, described in the text. Efficacy estimated from Effective Radiative Forcing $E_{ERF.}$ Efficacy estimated from Equivalent Effective Forcing $E_{EEF.}$ Efficacy estimated from α feedback parameter. The ratio of E_α estimated after 30 years to that estimated after 100 years.

(C) Exploring global-mean SST from AAMA scenario forcing using CRFs

Climate Change scenarios which include the effects of AAMA can be explored by assuming a relationship between global surface temperature anomalies and AAMA forcing levels. We use the AAMA scenarios of Golledge (2019) and DeConto and Pollard (2016), summarised in Figure S1a, and employ linear convolution theory. We estimate the degree of AAMA cooling for a given change in surface temperature. A 21st century GHG+AAMA scenario is inferred by comparing the amelioration of warming due to AAMA relative to IPCC surface temperature projections (O'Neil et al., 2016).

To take account of the fact that AAMA forcing over the 21st century is not likely to be small perturbation about a constant reference amplitude, a staggered linear convolution theory (LCT) approach is employed. This is achieved by breaking the time-series into segments of similar melt rate (i.e. 0-1000, 1000-2000, 2-4000, 4000-8000, 8000-20000) and assuming that the response to AAMA is linear within each one. The AAMA contribution to temperature change for each segment is obtained using the LCT approach described by Marshall et al (2014), Rye et al., (2020). This is then subtracted from the relevant RCP surface temperature scenario (O'Neil et al., 2016). Such an approach is only able to provide a guide but the results are of interest and shown in Figure S1.

Using RCP8.5 and the AAMA scenario of Golledge et al., (2019) (Figure S1b), we see that by 2050, AAMA reduces the impact of GHG warming by between 10 to 30%, (difference between the GHG scenario, thick red line, and GHG + AAMA scenario blue shaded area, at 2050). Using RCP8.5 and the much larger AAMA scenario of Deconto and Pollard et al, (2016) (Figure S1c) we find that by 2050 AAMA reduces the impact of GHG warming by between 20 to 40%. The difference in AAMA cooling between the two scenarios is rather small, particularly when one notes that the Deconto and Pollard et al, (2016) AAMA forcing is the largest by a factor of 3 by mid-century. The AAMA cooling impact of 10 to 30% appropriate for the Golledge et al., (2019) melt rate scenario is therefore preferred. This is the range quoted in the Abstract.

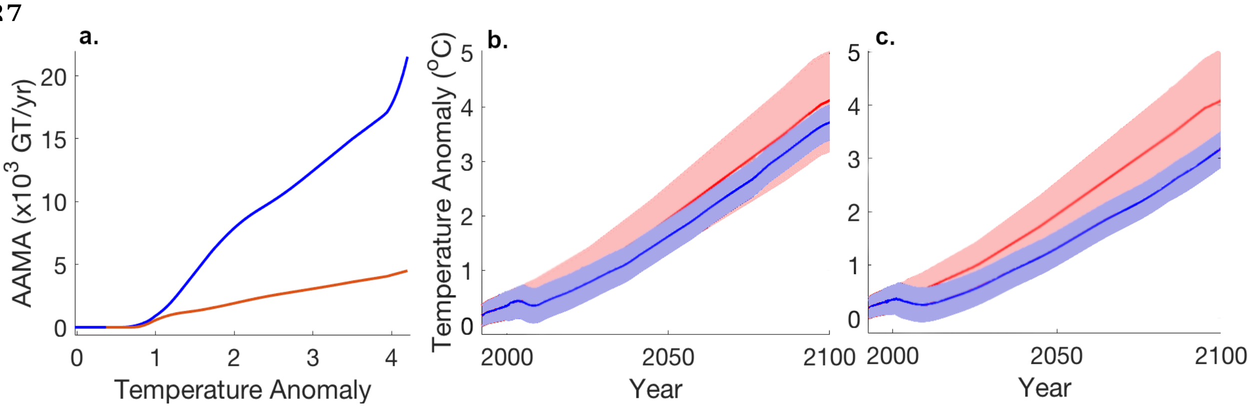

Figure S1 | Climate Change Scenarios based on CRFs and linear convolution theory. a. The projected AAMA as a function of temperature anomaly for the high-AAMA scenario of DeConto and Pollard (2016; blue) and the lower-AAMA scenario of Golledge (2019; red). b-c. Climate Change scenarios. Red shading: CMIP-5 multi-model spread temperature projections for RCP8.5. Blue shading: AAMA modified scenario. b. for the Golledge (2019) AAMA scenario. c. for DeConto and Pollard (2016). b. and c. are estimated using a climate response functions shown in Figure 2 and linear convolution theory.

Finally, it should be noted that, as found in Schloesser et al., (2019), the potency of melt water forcing may be diminished by as much as 50% if both both GHG and AAMA forcing are active. Our focus in this paper has been to elucidate how glacial meltwater changes can affect the global climate in isolation of other effects. A range of online scenarios when both forcings are simultaneously active is clearly needed to take account of such non-linear interactions.

References

Griffies, S.M., 1998. The Gent–McWilliams skew flux. *Journal of Physical Oceanography*, *28*(5), pp.831-841.

Large, W.G. and Gent, P.R., 1999. Validation of vertical mixing in an equatorial ocean model using large eddy simulations and observations. *Journal of Physical Oceanography*, *29*(3), pp.449-464.

Marshall, J., Armour, K.C., Scott, J.R., Kostov, Y., Hausmann, U., Ferreira, D., Shepherd, T.G. and Bitz, C.M., 2014. The ocean's role in polar climate change: asymmetric Arctic and Antarctic responses to greenhouse gas and ozone forcing. *Philosophical Transactions of the Royal Society A: Mathematical, Physical and Engineering Sciences*, *372*(2019), p.20130040.

Miller, R.L., Schmidt, G.A. and Shindell, D.T., 2006. Forced annular variations in the 20th century intergovernmental panel on climate change fourth assessment report models. *Journal of Geophysical Research: Atmospheres*, *111*(D18).

Schmidt, G.A., Ruedy, R., Hansen, J.E., Aleinov, I., Bell, N., Bauer, M., Bauer, S., Cairns, B., Canuto, V., Cheng, Y. and Del Genio, A., 2006. Present-day atmospheric simulations using GISS ModelE: Comparison to in situ, satellite, and reanalysis data. *Journal of Climate*, *19*(2), pp.153-192.

Tournadre, J., Bouhier, N., Girard‐Ardhuin, F. and Rémy, F., 2016. Antarctic icebergs distributions 1992–2014. *Journal of Geophysical Research: Oceans*, *121*(1), pp.327-349.

Visbeck, M., Marshall, J., Haine, T. and Spall, M., 1997. Specification of eddy transfer coefficients in coarse-resolution ocean circulation models. *Journal of Physical Oceanography*, *27*(3), pp.381-402.